Simulations of SASI, turbulence, and magnetic field amplification

INT Program INT-12-2a: Core-Collapse Supernovae: Models and Observable Signals

Eirik Endeve

Funding: DoE Office of Advanced Scientific Computing Research
and Office of Nuclear Physics

Computing resources provided by DoE through the INCITE program

OAK RIDGE NATIONAL LABORATORY

Managed by UT-Battelle for the Department of Energy

Turbulence and Magnetic Fields from SASI

Objectives:

- Does turbulence develop from the SASI?
  - What are the characteristics of SASI-driven turbulence?
  - Does turbulence result in nonlinear SASI saturation? (e.g., Guilet et al. 2010, *ApJ*, **713**, 1350)
- Does SASI-driven turbulence result in magnetic field amplification?
  - What are the characteristics of SASI-driven magnetic field amplification?
- Do amplified magnetic fields change characteristics of the SASI?
  - Implications for the explosion mechanism of CCSNe?
- Do SASI + B-fields impact observables associated with CCSNe?
  - Implications for proto-neutron star magnetic fields?

Endeve, Cardall, Budiardja, & Mezzacappa (2010), *ApJ*, **713**, 1219

Endeve, Cardall, Budiardja, Beck, Bejnood, Toedte, Mezzacappa, & Blondin (2012), *ApJ*, **751**, 26

Endeve, Cardall, Budiardja, Mezzacappa, & Blondin (2012), *Physica Scripta*, in press (arXiv:1203:3748)

Turbulence and Magnetic Fields from SASI

Methods:

- High-resolution magnetohydrodynamic (MHD) simulations
  - Multiple models (vary rotation rate and initial field strength)
  - Grids up to 1280^3 zones
  - CPU time at OLCF provided by DoE through the INCITE program
- Idealized semi-analytic initial condition
  - Blondin & Mezzacappa (2007), Nature, 445, 58 **+ weak B-field**
- Analysis includes Fourier decomposition
  - Kinetic, Magnetic, and Enstrophy spectra

Endeve, Cardall, Budiardja, & Mezzacappa (2010), *ApJ*, **713**, 1219

Endeve, Cardall, Budiardja, Beck, Bejnood, Toedte, Mezzacappa, & Blondin (2012), *ApJ*, **751**, 26

Endeve, Cardall, Budiardja, Mezzacappa, & Blondin (2012), *Physica Scripta*, in press (arXiv:1203:3748)

MHD Scheme in GenASiS

Finite volume method solves integral form of ideal MHD equations

$$\frac{\partial}{\partial t}\langle \mathbf{U}_{ijk}\rangle = -\frac{1}{V_{ijk}}\oint_{\partial V_{ijk}} \mathbf{F}(\mathbf{U},\mathbf{B})\cdot d\mathbf{A} + \langle \mathbf{S}_{ijk}(\mathbf{U},\Phi)\rangle$$

$$\frac{\partial}{\partial t}\langle B^x_{i+\frac{1}{2}jk}\rangle = -\frac{1}{A^x_{i+\frac{1}{2}jk}}\oint_{\partial A^x_{i+\frac{1}{2}jk}} \mathbf{E}(\mathbf{U},\mathbf{B})\cdot d\mathbf{L}$$

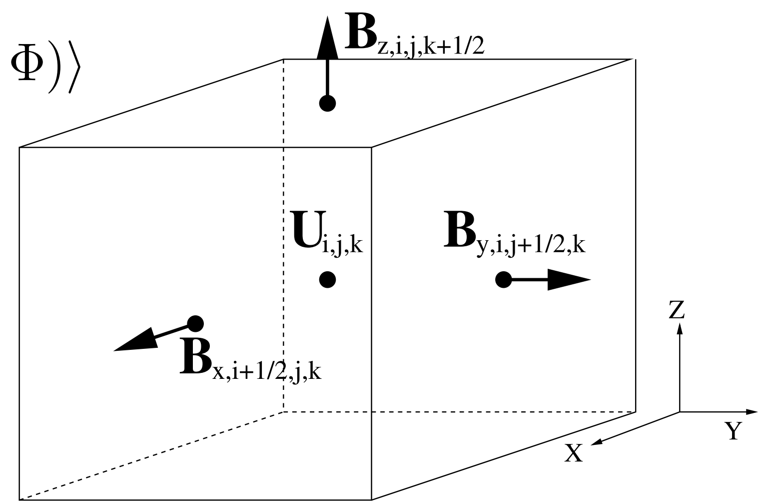

Second-order semi-discrete finite volume method

- Second-order in space through slope-limited linear interpolation
- HLL-type approximate Riemann solver ➔ flux + electric fields
- Constrained transport for divergence-free B-field update
- Second-order in time through TVD Runge-Kutta time integration

Kurganov et al. (2001), *SIAM, J.Sci.Comput.*, **23**, 707
Londrillo & Del Zanna (2004), *JCP*, **195**, 17
Endeve et al. (2012), *J. Phys.: Conf. Ser.*, in press (arXiv:1203:3385)

MHD Scheme in GenASiS

Second-order convergence for smooth problems: Circularly polarized Alfven wave

Table 1. L_1-error and convergence rate for the circularly polarized Alfvén wave test.

	TW ($t_f = 1$)		SW ($t_f = 1$)		TW ($t_f = 5$)		SW ($t_f = 5$)	
N_x	$L_1(B_z)$	Rate	$L_1(B_z)$	Rate	$L_1(B_z)$	Rate	$L_1(B_z)$	Rate
32	1.373E-01	–	2.279E-01	–	4.974E-01	–	7.361E-01	–
64	5.196E-02	−1.40	8.629E-02	−1.40	1.395E-01	−1.83	2.144E-01	−1.78
128	1.433E-02	−1.86	2.535E-02	−1.77	5.053E-02	−1.46	8.700E-02	−1.30
256	3.625E-03	−1.98	6.842E-03	−1.89	1.483E-02	−1.77	2.754E-02	−1.66
512	9.085E-04	−2.00	1.760E-03	−1.96	3.945E-03	−1.91	7.782E-03	−1.82
1024	2.242E-04	−2.02	4.491E-04	−1.97	1.015E-03	−1.96	2.059E-03	−1.92

First-order convergence for problems with discontinuities: Orzag-Tang vortex

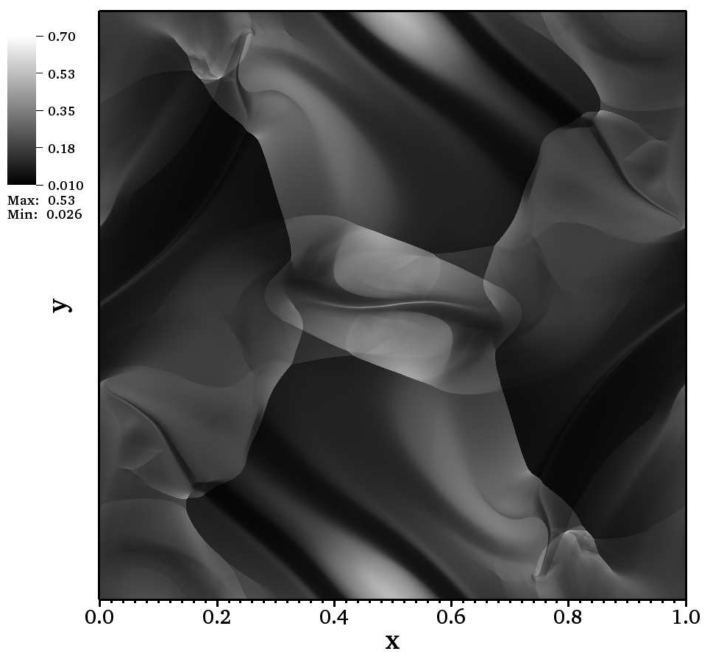

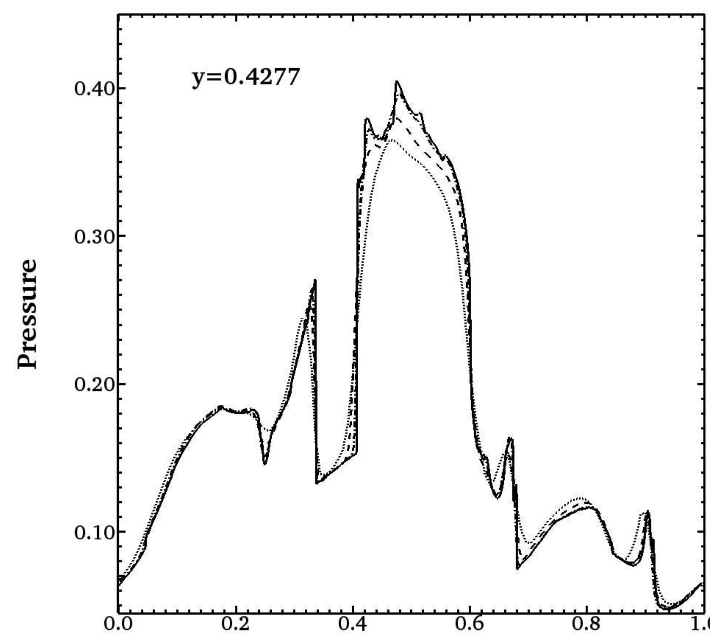

Turbulence from Spiral SASI Modes

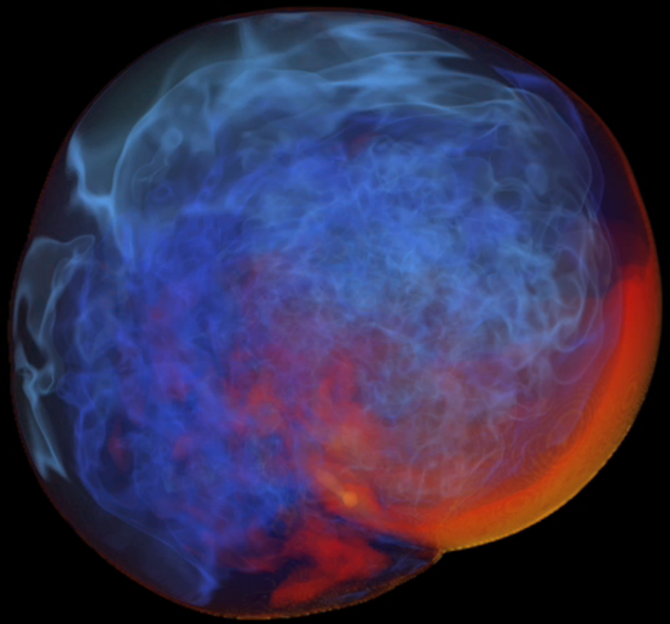

time=832 ms

- SASI Spiral modes emerge favorably
- Turbulence driven by supersonic shear flows
- Postshock flow: Supersonic **driving** component +subsonic **turbulent (volume filling)** component

Supersonic flows contribute mostly to the wings of the PDF for v_x

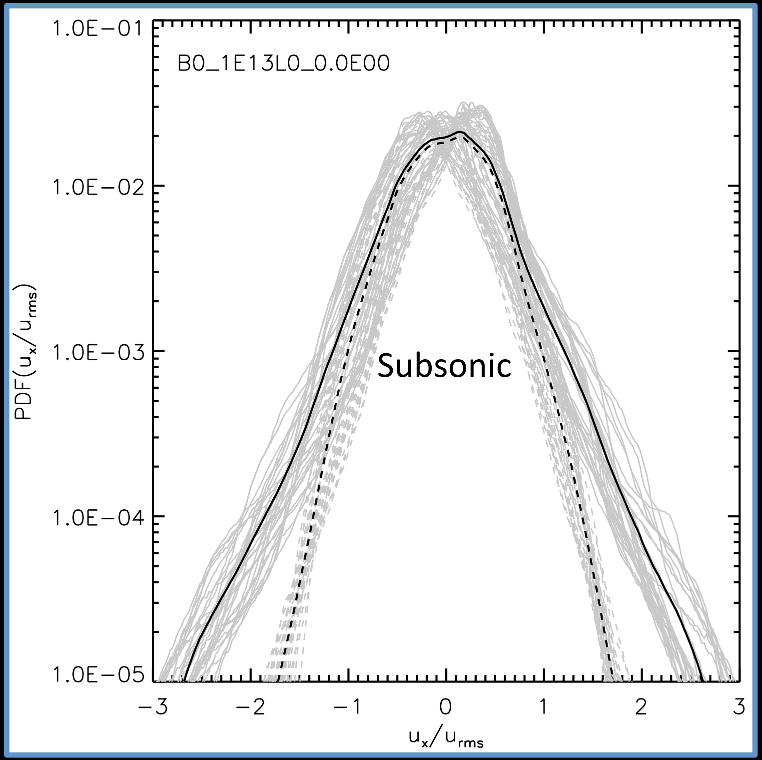

Turbulence from Spiral SASI Modes

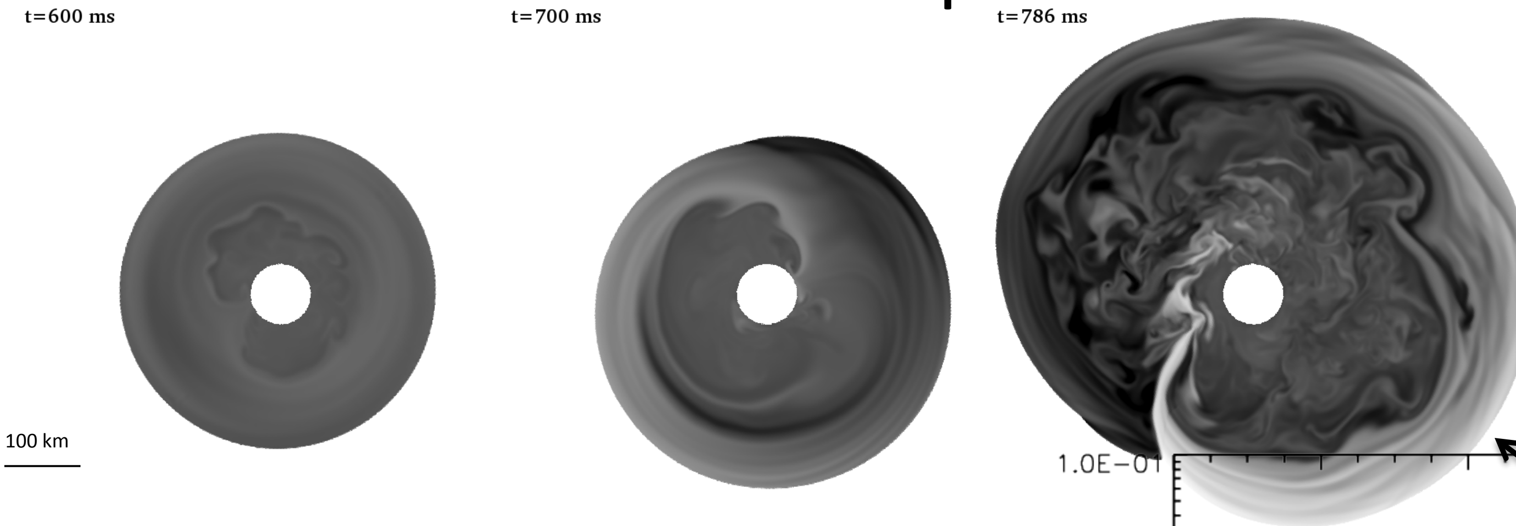

Significant post-shock turbulence at saturation

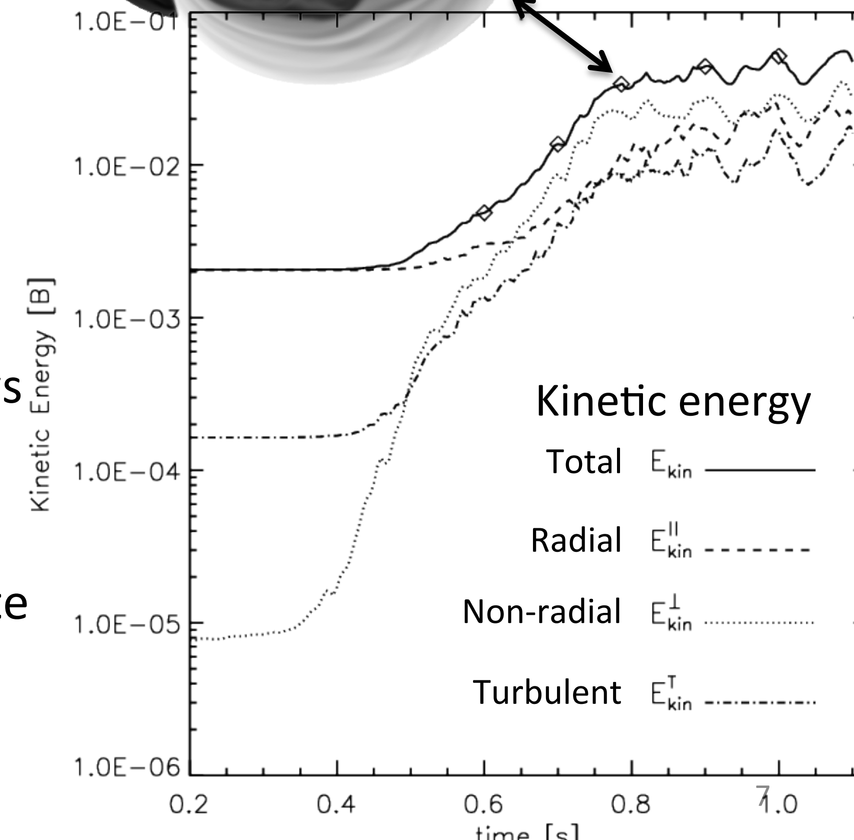

- Turbulence develops from secondary instabilities (e.g., KH) in the shear layer induced by the spiral SASI mode
- Non-radial and turbulent kinetic energy grows rapidly during nonlinear SASI development
- Radial and non-radial kinetic energy in equipartition during turbulent, saturated state (similar to turbulence from neutrino-driven convection; Murphy et al. arXiv:1205.3491)

Fourier Decomposition of Simulation Results

For any vector field we compute Fourier amplitudes (using FFTW library)

$$\hat{\mathbf{f}}(\mathbf{k}) = \frac{1}{V_L} \int_{V_L} \mathbf{f}(\mathbf{x}) \times \exp(i\mathbf{k} \cdot \mathbf{x})\, dV$$

Define the spectral energy density in *k*-space shell

$$\hat{e}(k) = \frac{1}{2} \int_{k\text{-Shell}} |\hat{\mathbf{f}}|^2\, k^2 d\Omega_k$$

$$\boxed{\int_0^\infty \hat{e}\, dk = \frac{1}{2} \int_{V_L} |\mathbf{f}|^2\, dV}$$

$$\mathbf{f}(\mathbf{x}) = \sqrt{\rho}\,\mathbf{u},\ \mathbf{u},\ \boldsymbol{\omega},\ \mathbf{B} \longrightarrow \hat{e}_{\mathrm{kin}},\ \hat{e}_{\mathbf{u}},\ \hat{e}_{\boldsymbol{\omega}},\ \hat{e}_{\mathrm{mag}}$$

(i.e., kinetic energy, specific kinetic energy, enstrophy, and magnetic energy spectra)

Nonlinear Saturation of SASI due to Turbulence?

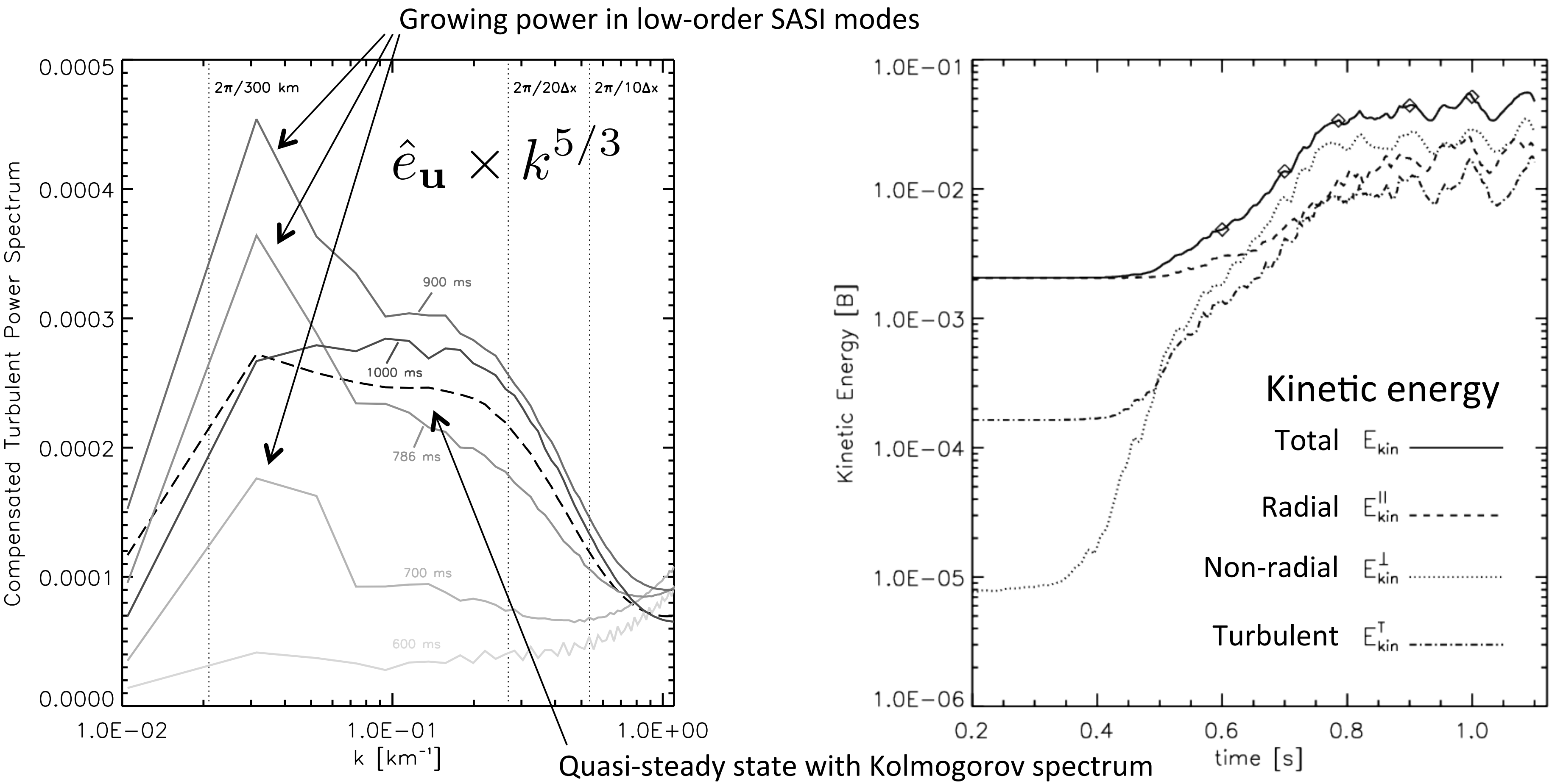

- SASI saturation coincides with development of turbulence
- Quasi-steady state with Kolmogorov spectrum develops
  - Accretion-powered large-scale flows cascade to smaller scales and dissipate (numerically)

Impact of Numerical Resolution

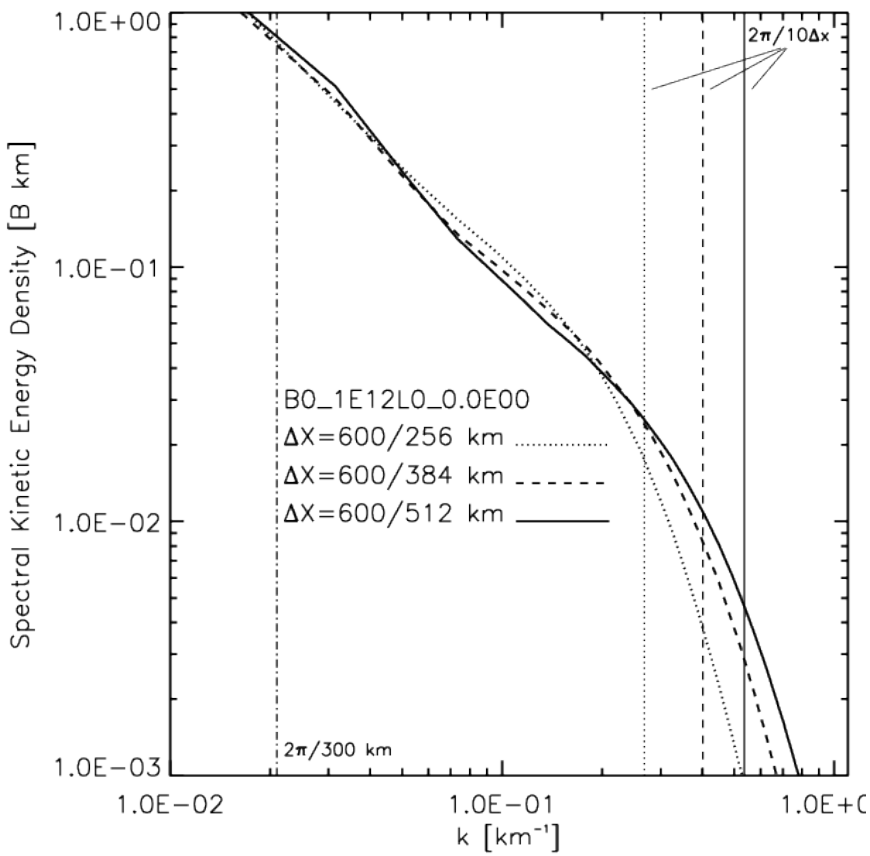

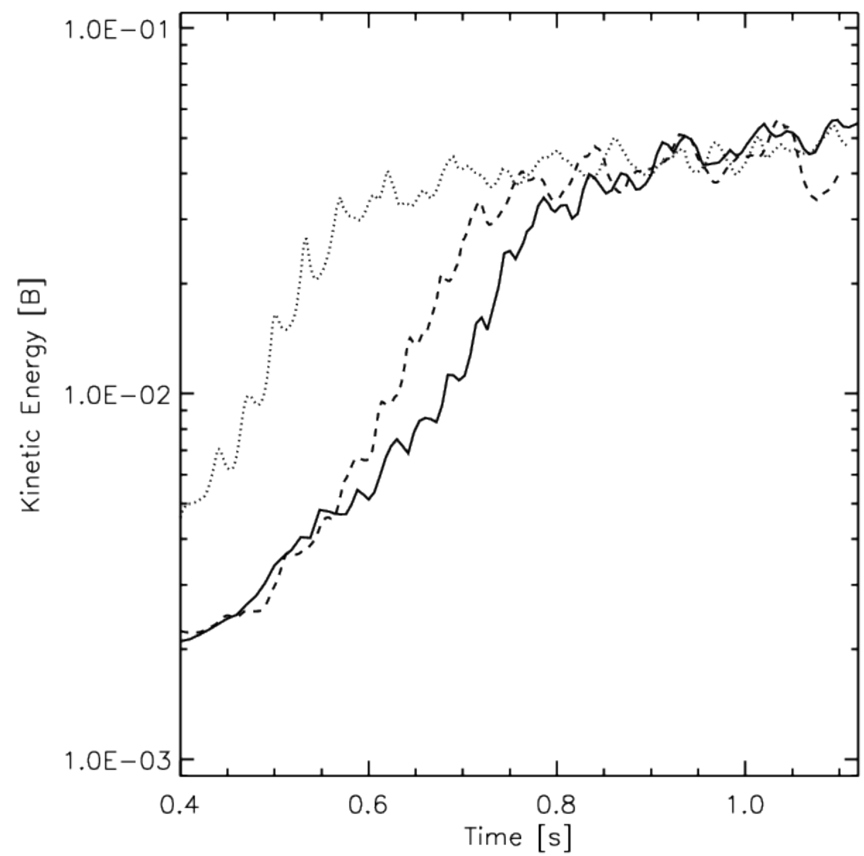

- Kinetic energy Spectrum extends to larger *k*-values for higher resolution
  - Numerical dissipation causes spectrum to decrease faster than $k^{-5/3}$
- No impact on saturation level of kinetic energy

  (earlier onset of nonlinear SASI for lowest resolution model)

Non-Helical Turbulence from SASI

PDF: relative kinetic helicity

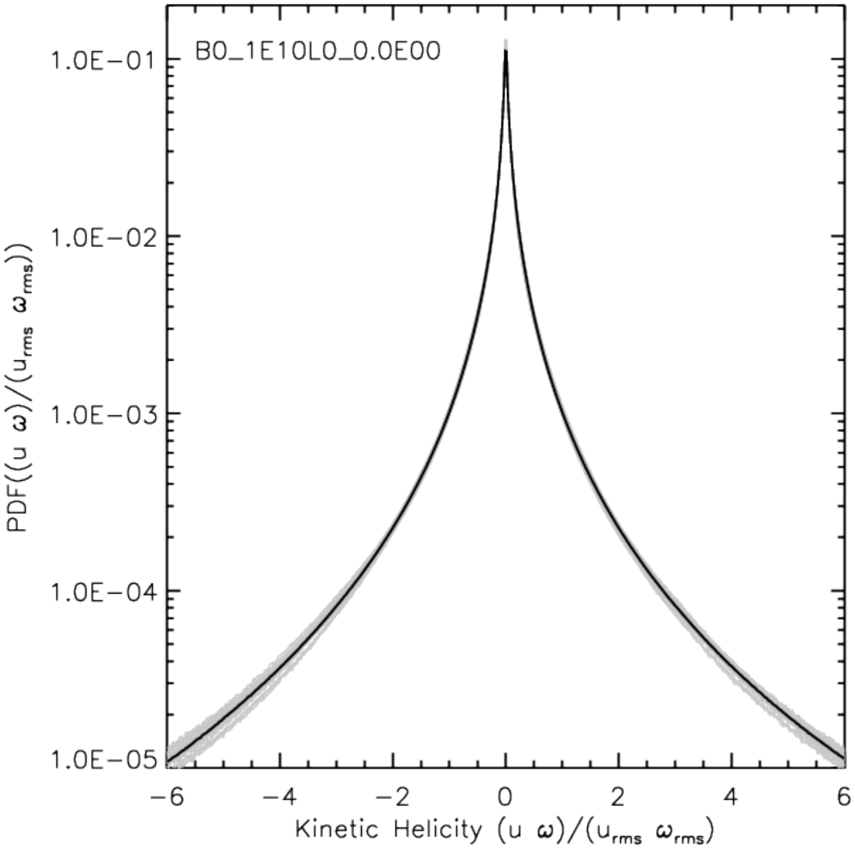

Relative kinetic helicity

$$h_{\mathrm{kin}} = \frac{\mathbf{u}\cdot\boldsymbol{\omega}}{u_{\mathrm{rms}}\,\omega_{\mathrm{rms}}}$$

Net kinetic helicity small in SASI simulations

$$\left|\int_{-\infty}^{+\infty} h_{\mathrm{kin}}\,\mathrm{PDF}(h_{\mathrm{kin}})\,dh_{\mathrm{kin}}\right| < 10^{-3}$$

Important for magnetic field amplification!

Non-helical turbulence: small-scale dynamo (Haugen et al. 2004)

Helical Turbulence: Large-scale dynamo (inverse cascade; Meneguzzi et al. 1981, Brandenburg 2001, Blackman 2012)

SASI-driven turbulence: *B-field amplification via efficient small-scale dynamo*

− Similar to convectively driven turbulence (Brandenburg et al. 1996, *J. Fluid Mech.*, **306**, 325)

Kinetic helicity may increase with sufficient differential rotation

Turbulent Magnetic Field Amplification

Post-shock magnetic energy

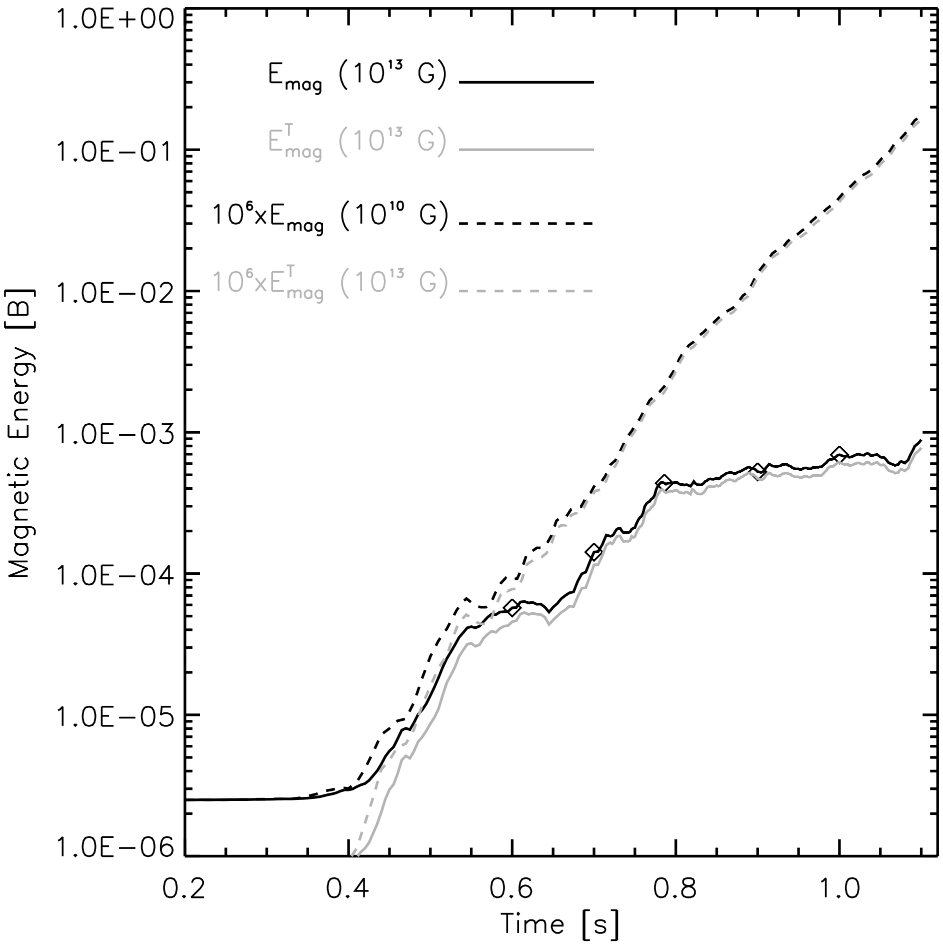

Total magnetic energy

$$E_{\rm mag} = \int_{V_{\rm Sh}} \frac{\mathbf{B}\cdot\mathbf{B}}{2\mu_0}\, dV$$

Growth due to turbulent small-scale dynamo

$$E^{\rm T}_{\rm mag} = \int_{k^{\rm T}}^{\infty} \hat{e}_{\rm mag}\, dk$$

$$\lambda < 2\pi/k_{\rm T} \approx 60 \text{ km}$$

- B-fields grow exponentially
  - **$B_0=10^{10}$ G:** steady growth, **τ≈65 ms**, **$B_0=10^{13}$ G:** growth tapers off, **E_{mag}≈5×10^{47} erg**
  - Growth rate underestimated by numerical simulations!

Magnetic field magnitude

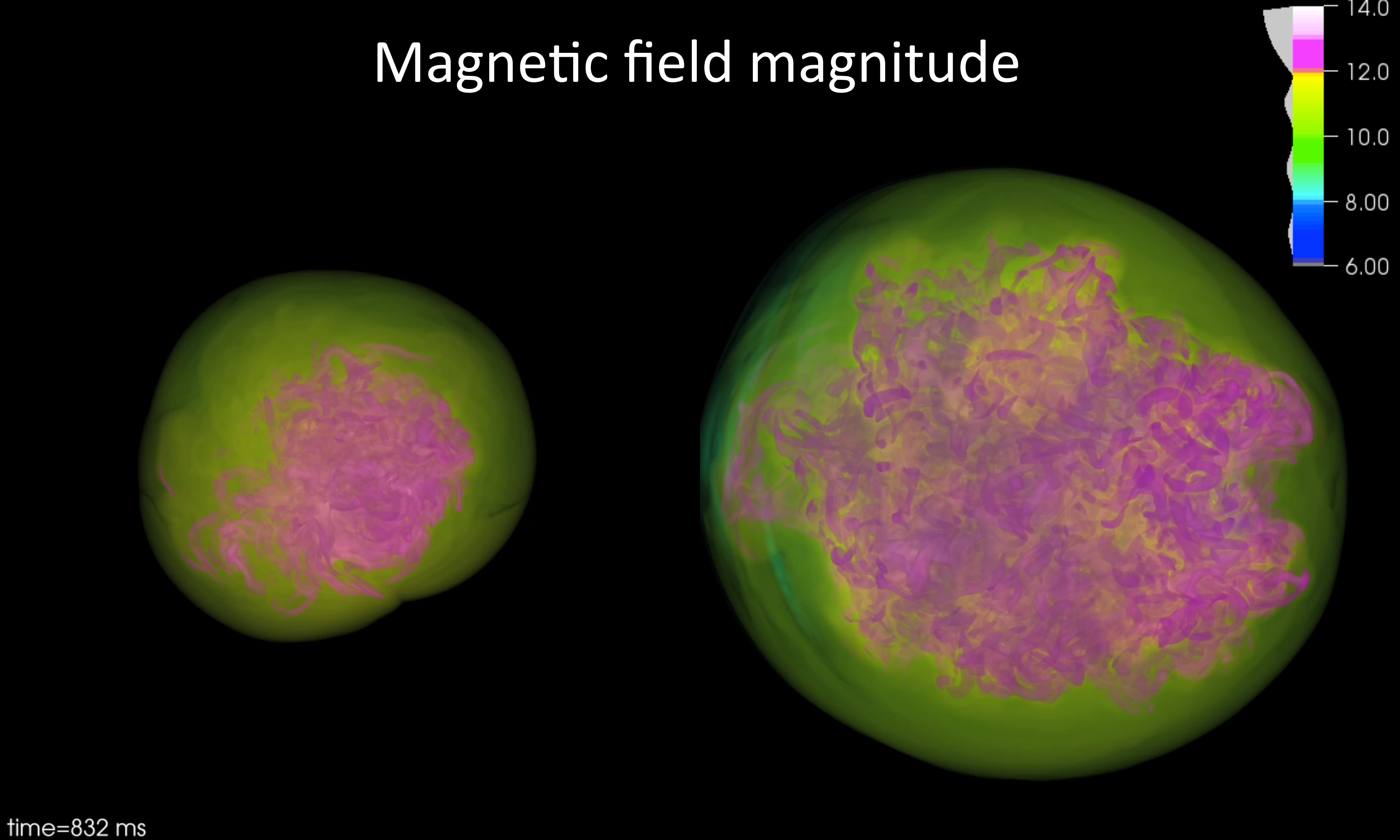

Saturation of Magnetic Energy

$e_{mag}/e_{kin}=(v_A/u)^2$

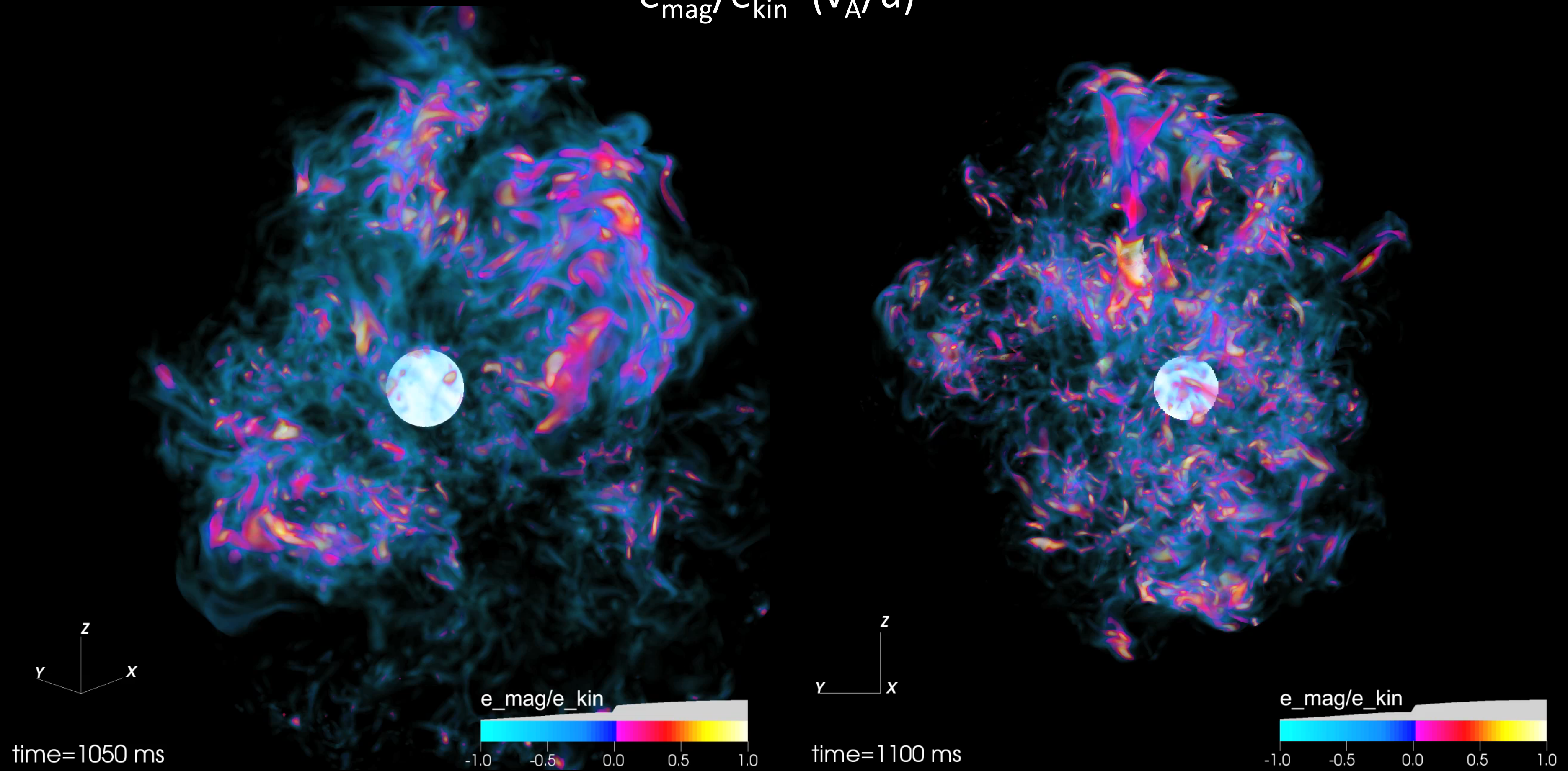

- Magnetic field displays spatial and temporal intermittency

Spectral Evolution of Magnetic Energy

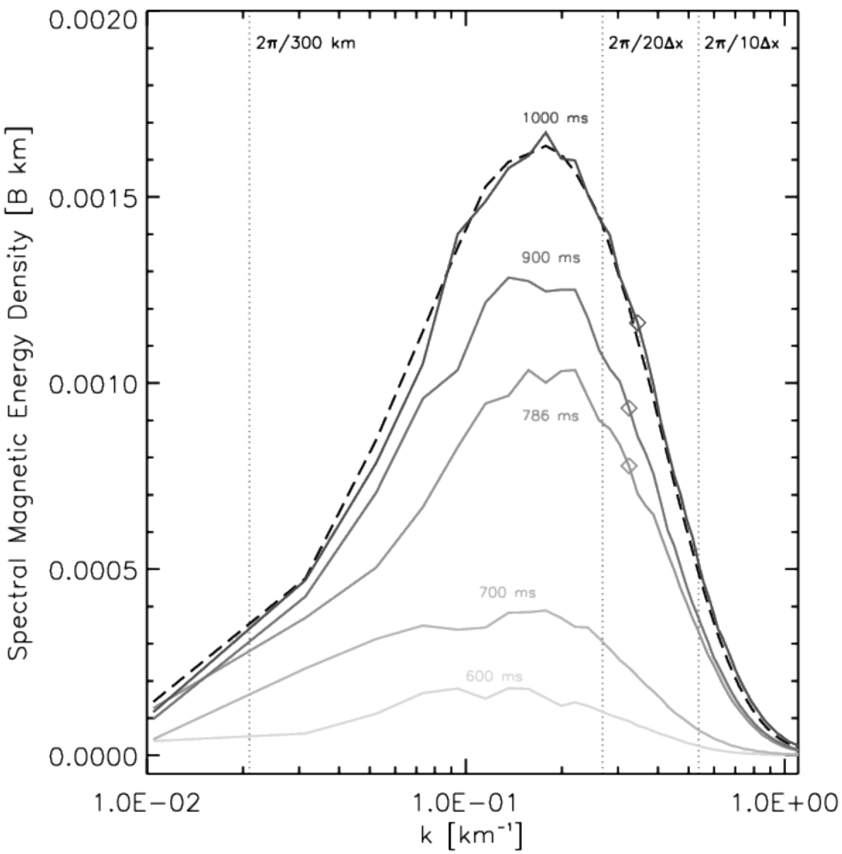

Magnetic spatial scale (resolution dependent)

$$\bar{\lambda}_{\rm mag} = 2\pi \frac{\int_0^\infty \widehat{e}_{\rm mag}(k)\, dk}{\int_0^\infty k \widehat{e}_{\rm mag}(k)\, dk} \approx 20 \text{ km}$$

Turbulent kinetic energy

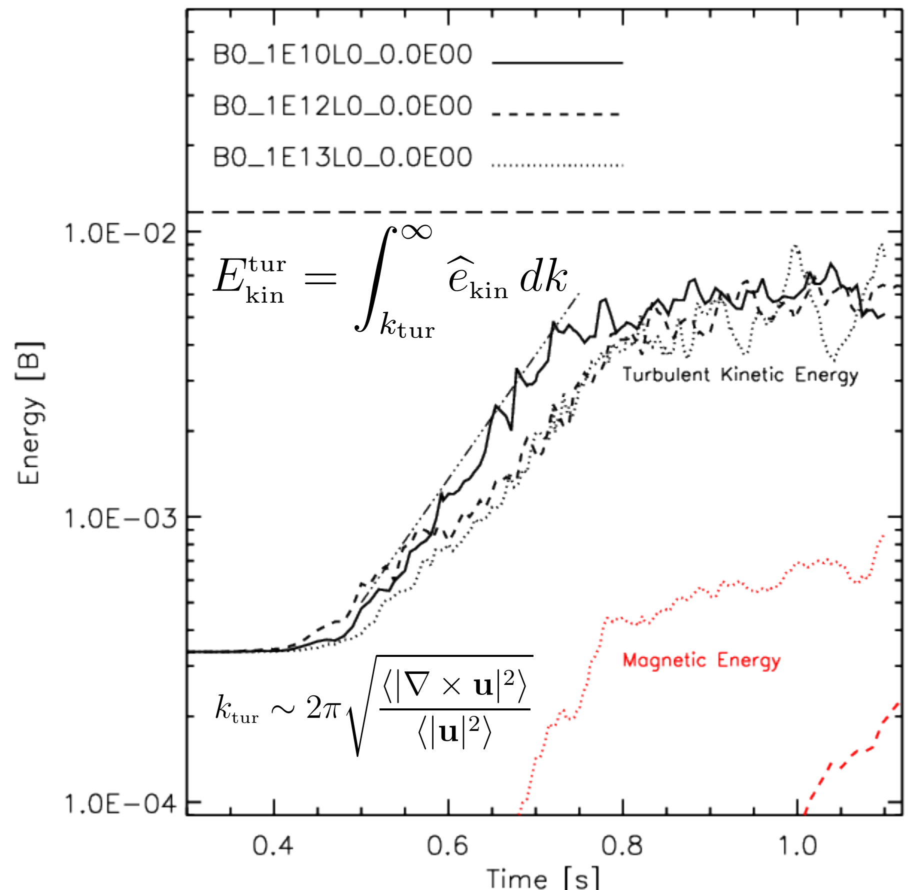

Turbulent rms velocity

$$u_{\rm rms} = \left(\frac{2E_{\rm kin}^{\rm tur}}{M_{\rm Sh}} \right)^{1/2} \approx 4 \times 10^3 \text{ km s}^{-1}$$

$$\tau \sim \bar{\lambda}_{\rm mag}/u_{\rm rms} \approx 5 \text{ ms}$$

Amplification of Magnetic Fields

$$\frac{\partial}{\partial t}\left(\frac{\mathbf{B}\cdot\mathbf{B}}{2\mu_0}\right) = \frac{1}{\mu_0}\mathbf{B}\cdot\left[\underbrace{(\mathbf{B}\cdot\nabla)\,\mathbf{u}}_{\text{stretching}} - (\mathbf{u}\cdot\nabla)\,\mathbf{B} - \underbrace{\mathbf{B}\,(\nabla\cdot\mathbf{u})}_{\text{compression}}\right]$$

$$= -\nabla\cdot\mathbf{P} - \underline{\mathbf{u}\cdot(\mathbf{J}\times\mathbf{B})}$$

- B-field amplified by ``stretching”

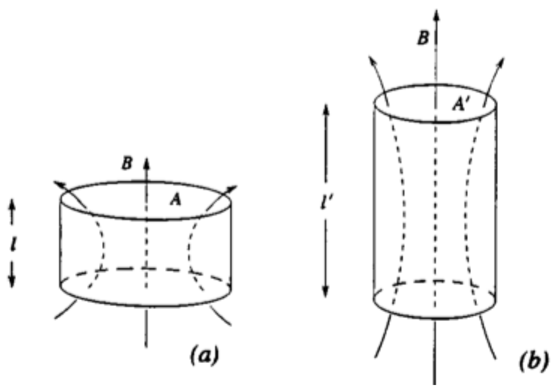

Ott (1998), Phys. Plasmas, 5, 1636

- Growth rate (inverse turnover time)

$$\Sigma_{\mathbf{J}\times\mathbf{B}} \approx 400\ \mathrm{s}^{-1}\left(\frac{u_{\rm rms}}{4000\ \mathrm{km\ s}^{-1}}\right)\left(\frac{\bar{\lambda}_{\rm mag}}{20\ \mathrm{km}}\right)^{-1}$$

  - Mismatch with simulations (15 s^{-1})!

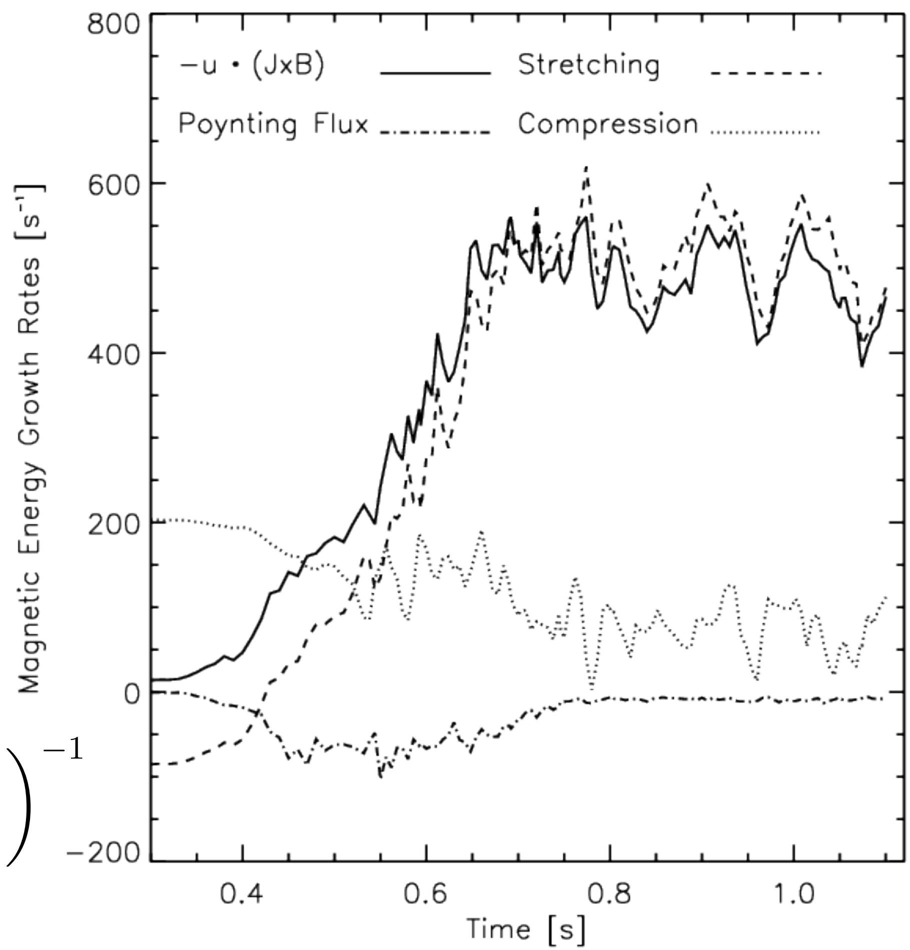

Effects of Finite (Numerical) Conductivity

$$\frac{\partial}{\partial t}\left(\frac{\mathbf{B}\cdot\mathbf{B}}{2\mu_0}\right) = -\nabla\cdot\mathbf{P} - \mathbf{u}\cdot(\mathbf{J}\times\mathbf{B}) - \frac{1}{\mu_0}\mathbf{B}\cdot\nabla\times(\eta\mathbf{J})$$

- Finite volume scheme mimics effect of finite conductivity to stabilize solution near discontinuities and sharp gradients
- Decrease in flux tube thickness halted by resistive dissipation
- Limits field amplification
- Magnetic energy growth rate severely underestimated

$$\Sigma \approx \Sigma_{\mathbf{J}\times\mathbf{B}} \times \left[1 - R_{\mathrm{m}}^{-1}\left(\frac{\bar{\lambda}_{\mathrm{mag}}}{\lambda_{\mathrm{d}}}\right)^2\right]$$

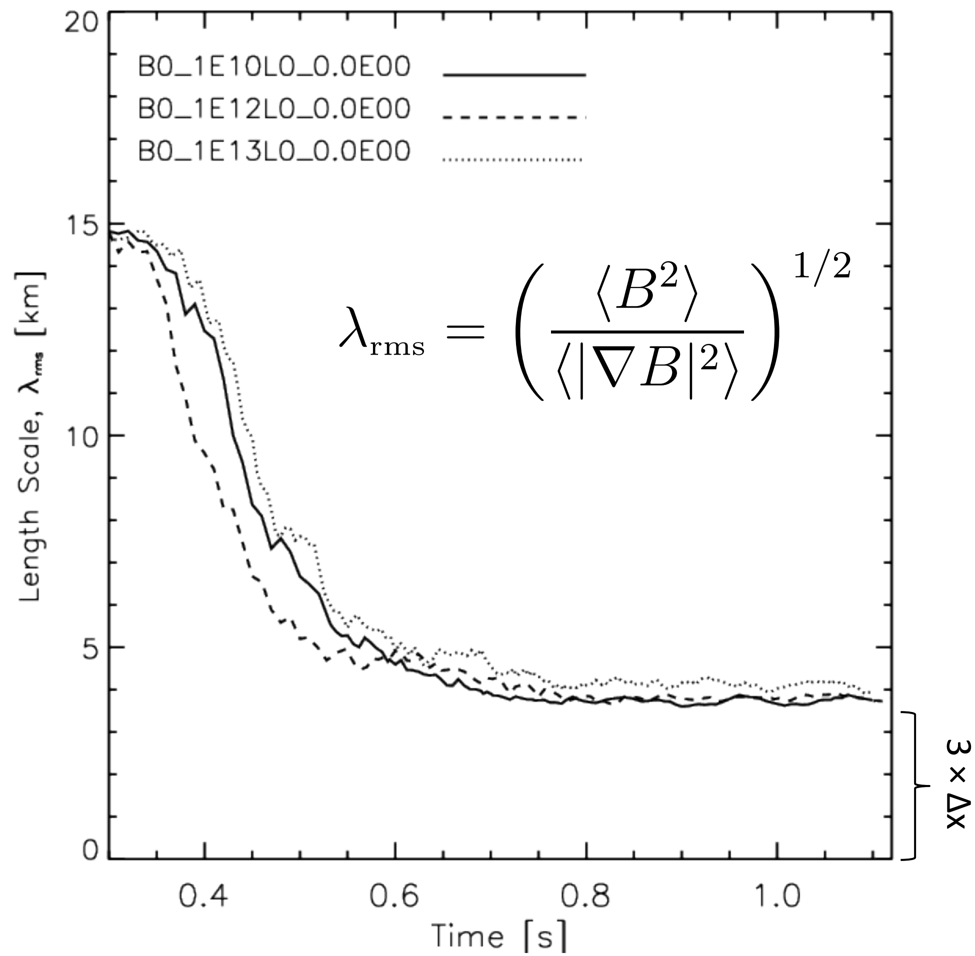

$$\lambda_{\mathrm{rms}} = \left(\frac{\langle B^2\rangle}{\langle|\nabla B|^2\rangle}\right)^{1/2}$$

Effects of Finite (Numerical) Conductivity

HLL electric field:

$$\langle E_z\rangle_p^n = \frac{\alpha_x^+\alpha_y^+\left[E_z^{\mathrm{SW}}\right]_p^n + \alpha_x^+\alpha_y^-\left[E_z^{\mathrm{NW}}\right]_p^n + \alpha_x^-\alpha_y^+\left[E_z^{\mathrm{SE}}\right]_p^n + \alpha_x^-\alpha_y^-\left[E_z^{\mathrm{NE}}\right]_p^n}{\left(\alpha_x^+ + \alpha_x^-\right)\left(\alpha_y^+ + \alpha_y^-\right)}$$

$$+ \frac{\alpha_x^+\alpha_x^-}{\left(\alpha_x^+ + \alpha_x^-\right)}\left(\left[B_y^{\mathrm{E}}\right]_p^n - \left[B_y^{\mathrm{W}}\right]_p^n\right)$$

$$- \frac{\alpha_y^+\alpha_y^-}{\left(\alpha_y^+ + \alpha_y^-\right)}\left(\left[B_x^{\mathrm{N}}\right]_p^n - \left[B_x^{\mathrm{S}}\right]_p^n\right),$$

- Finite volume scheme mimics effect of finite conductivity to stabilize solution near discontinuities and sharp gradients
- Contributes significantly to magnetic energy growth rate

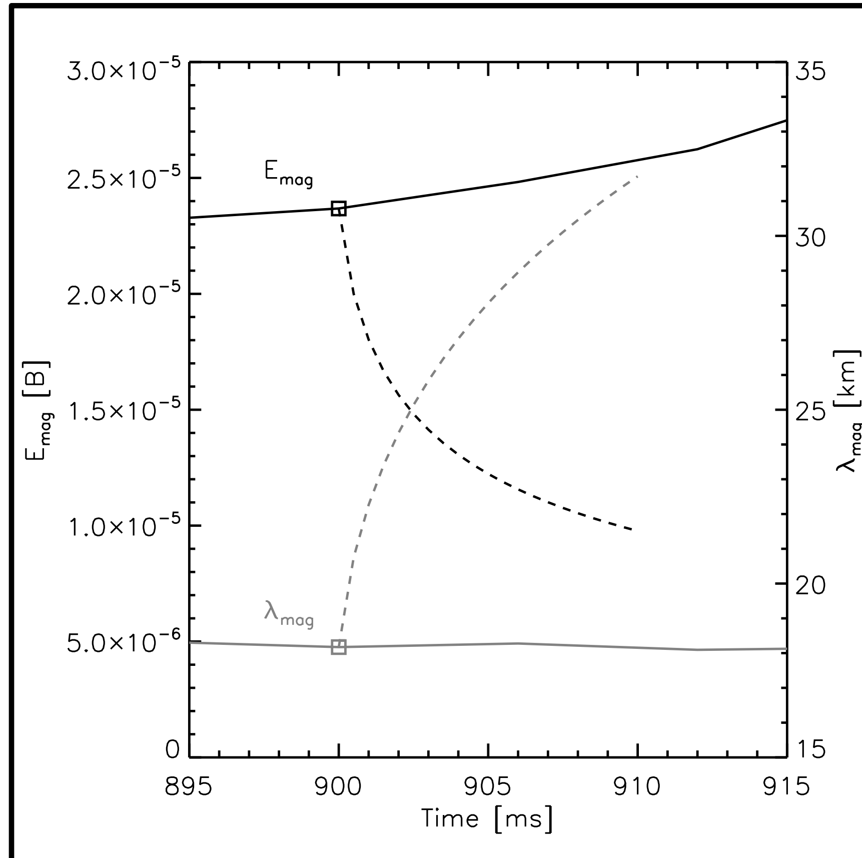

Simulations with Different Resolutions

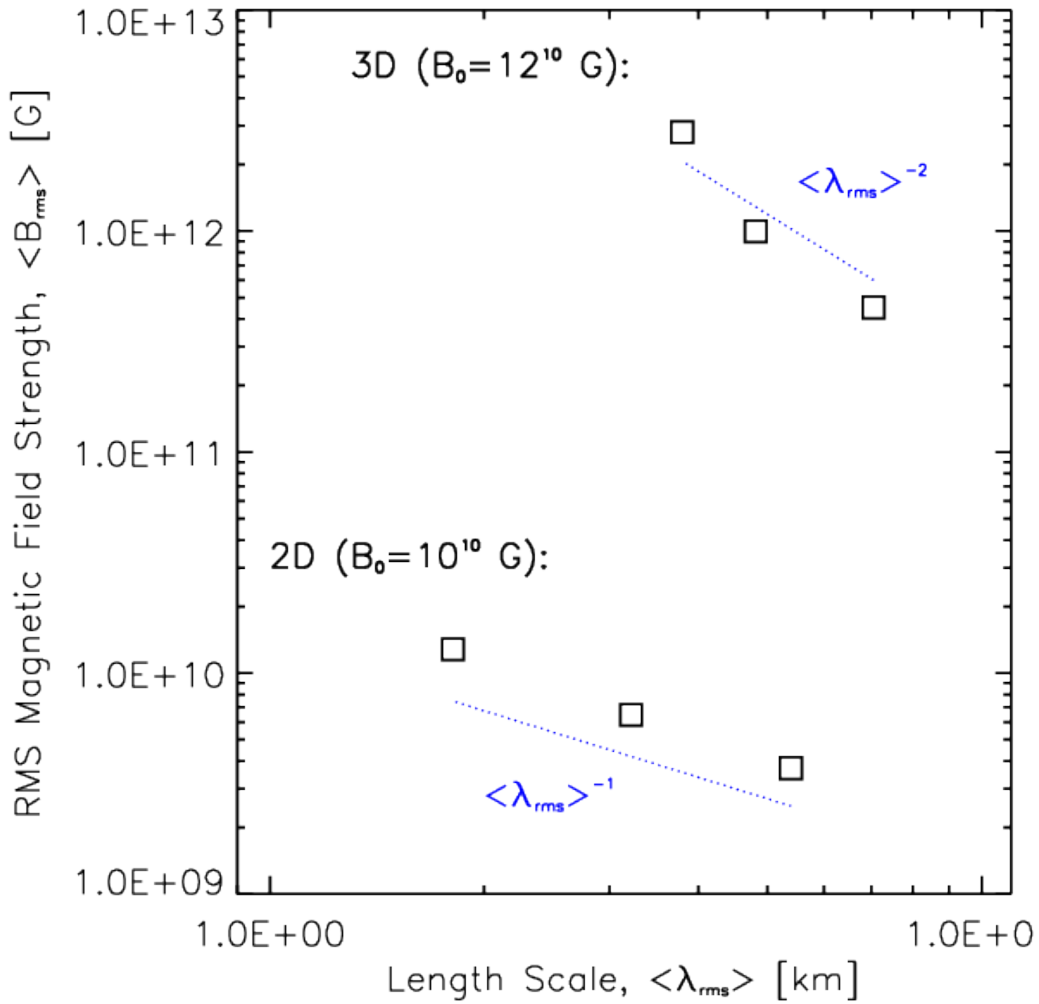

- Double grid resolution ➔ Magnetic energy increases by a factor ≈ 10^2
  - Growth rate also sensitive to spatial resolution

Impact of B-fields on Post-shock Flows

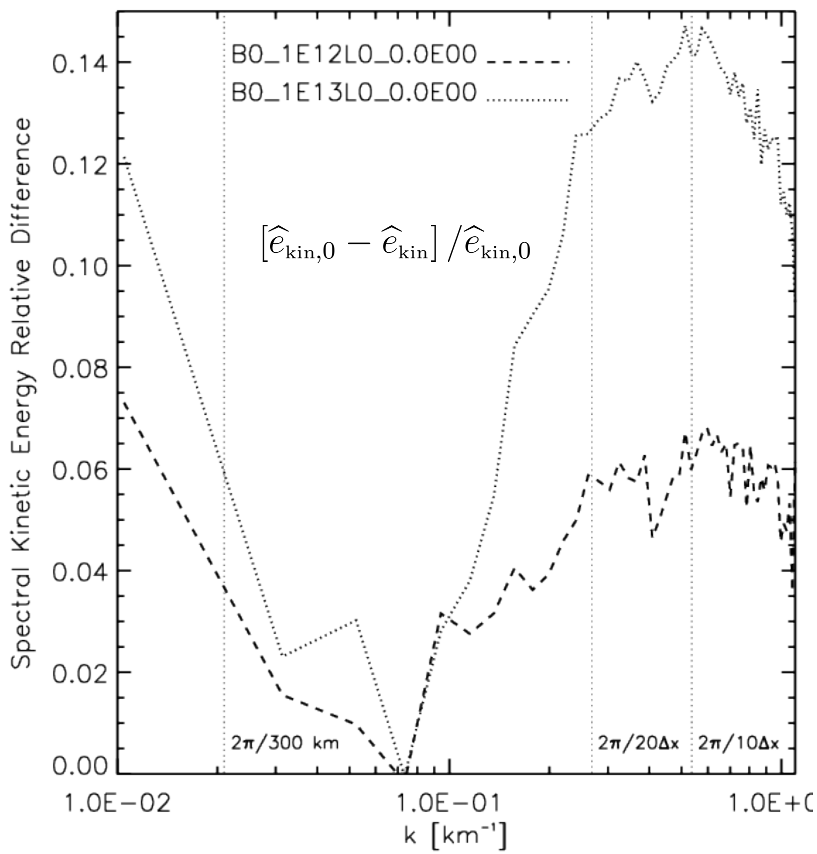

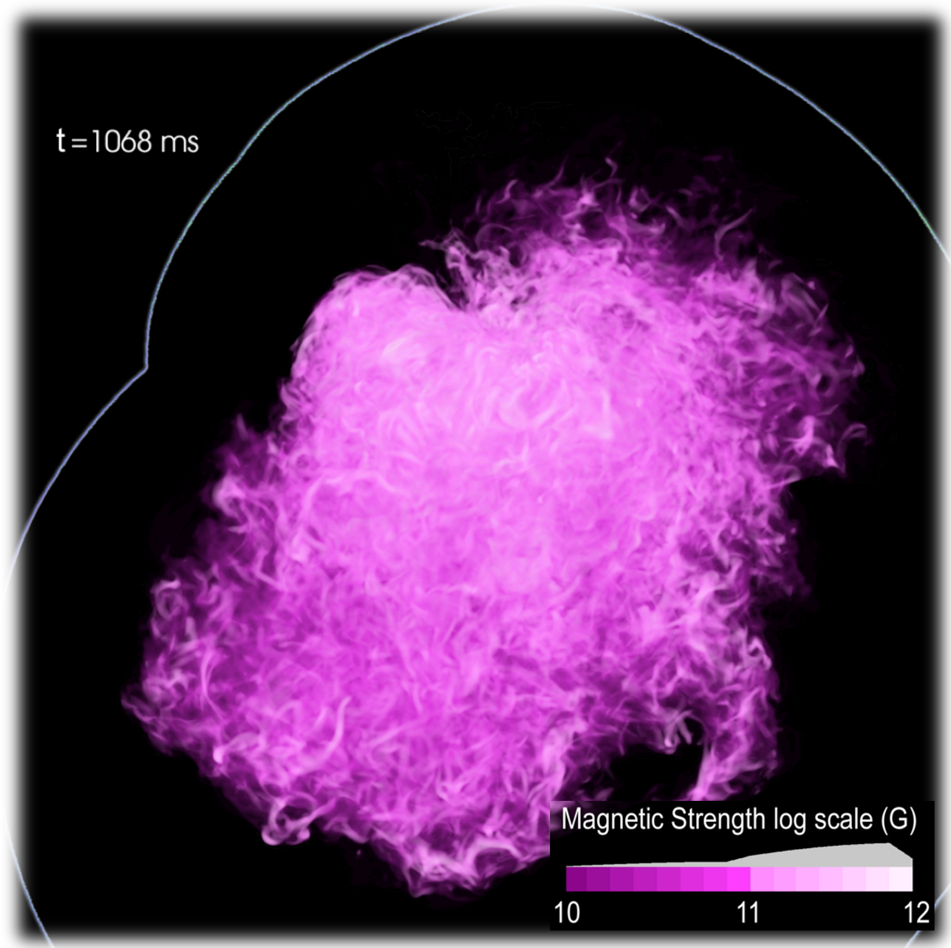

- Small-scale B-fields impact small-scale flows
- No impact on large scale dynamics detected

Implications for Proto-neutron Star Magnetization

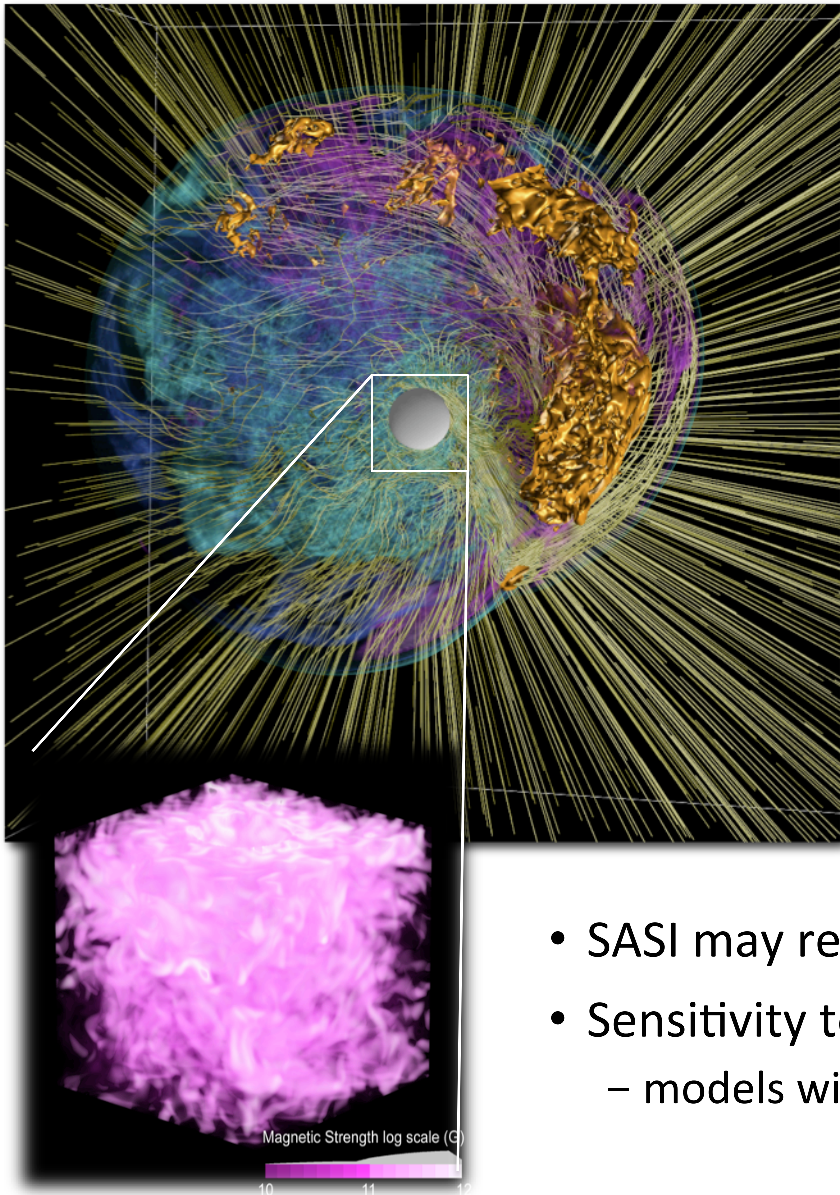

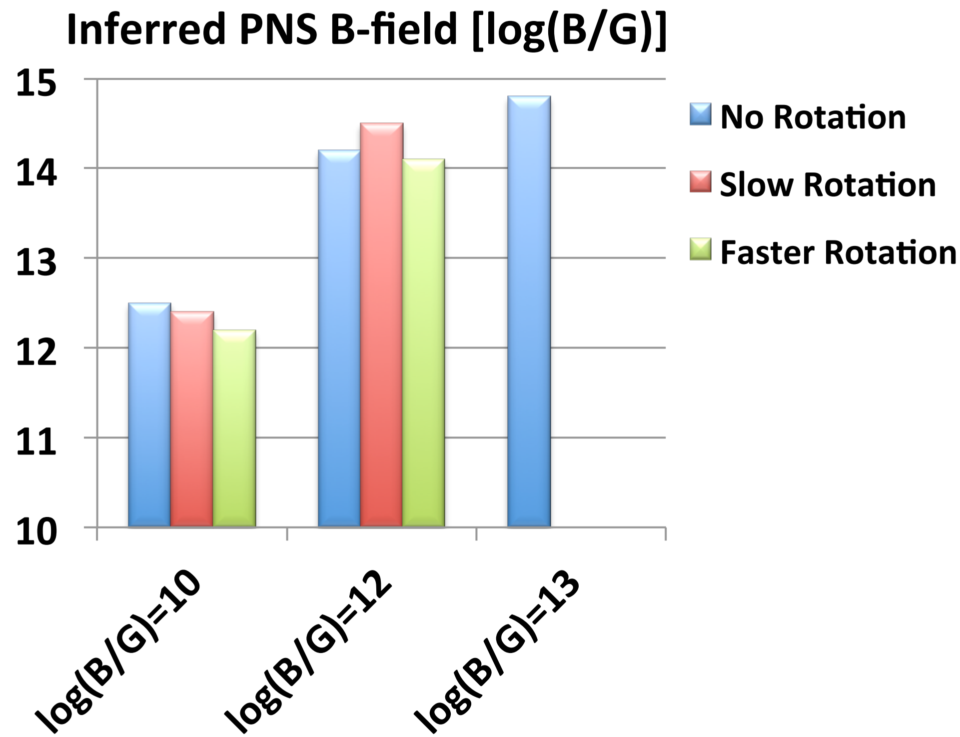

- SASI may result in PNS B-fields exceeding 10^{14} G
- Sensitivity to numerical resolution applies
  - models with weak initial fields saturate due to finite grid

Summary

- Nonlinear SASI drives vigorous turbulence below the shock
- Development of turbulence seems to result in SASI saturation
  - Turbulence feeds on power in low-order SASI modes
- Weak magnetic fields amplified exponentially
- Strong magnetic fields emerge and impact flows on small spatial scales
- SASI-induced B-fields not likely to play principal role in the explosion of CCSNe
  - Kinetic energy of explosion ≈ 1×10^{51}
  - Post-shock kinetic energy ≈ 5×10^{49}
  - Turbulent kinetic energy ≈ 5×10^{48} (only about 10% accessed by B-fields)
- SASI-induced magnetic fields may contribute nontrivially to PNS magnetization
  - Magnetic energy accreted onto the PNS > 10^{48} erg
  - Estimates suggest small scale B-fields in the 10^{14}-10^{15} G range

Are B-Fields Relevant for Non-rotating CCSNe?

- Idealized simulations offer proof of principle for efficient B-field amplification
- Must follow up with multi-physics simulations
  - Explicitly include PNS
  - Neutrino radiation transport

  (Explicitly include PNS and neutrino radiation transport: Computational cost increases dramatically!)
  - Does the spiral SASI mode play a central role?
  - Other field-amplification mechanisms also at play (α-Ω dynamo, MRI)
- Effects of finite grid resolution represents a challenge for global simulations
  - Magnetic energy growth rates underestimated
  - Flux-rope thickness (i.e., field strength) limited by size of grid cells
  - What happens at larger/realistic R_m (10^{16})?
  - Does modest rotation result in helical dynamo and large-scale B-fields?
  - Can we construct useful local simulations with guidance from global simulations?
- Details on evolution and impact of magnetic fields in CCSNe remain uncertain

Post-Shock Kinetic Energy from 2D Multi-Physics Runs

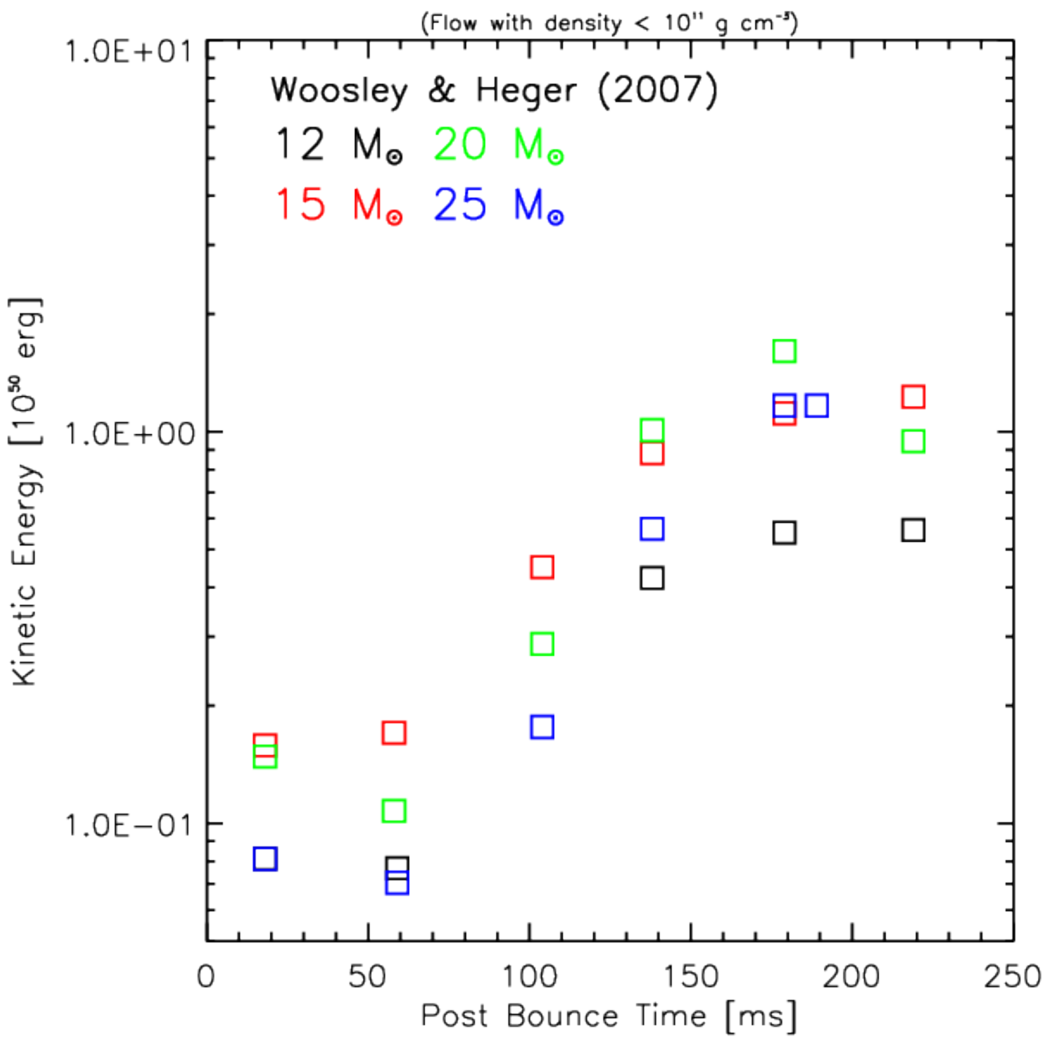

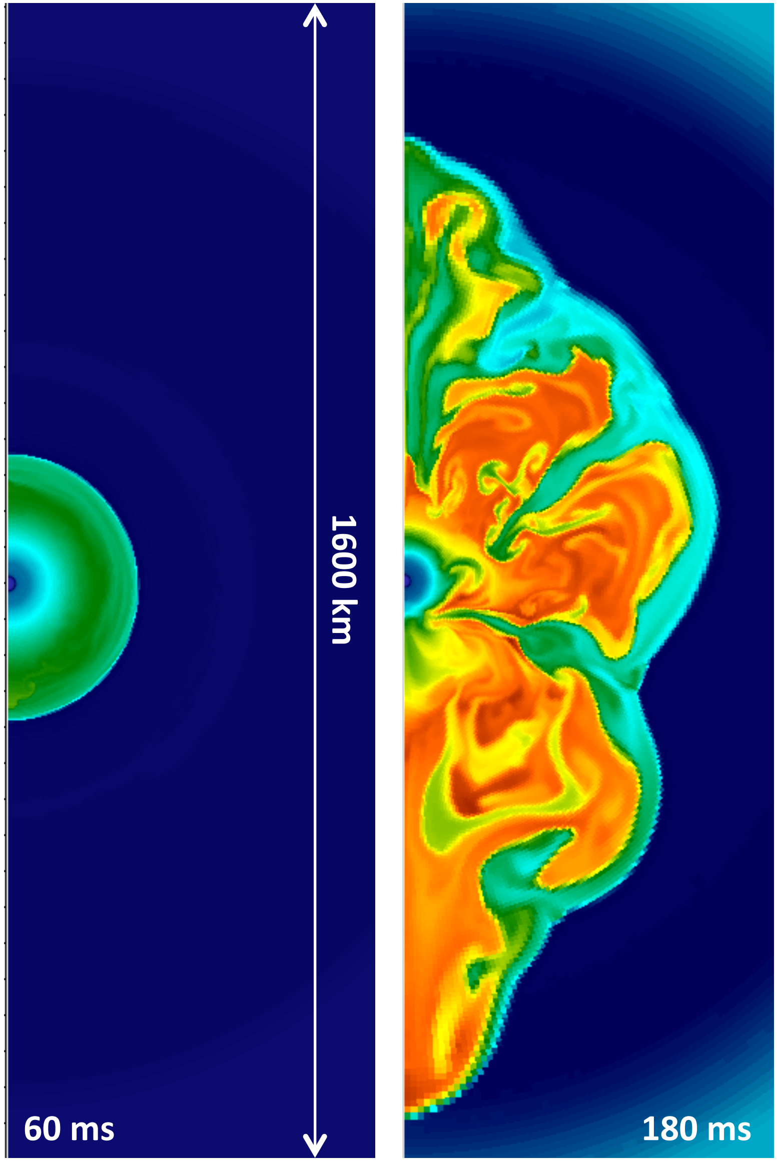

Bruenn et al. (2011), in preparation
Woosley & Heger (2007), Phys. Rep., 442, 269